To be published in "Structures and Buildings" (http://www.icevirtuallibrary.com/toc/jstbu/0/0)
Accepted on 05/10/2020
DOI: 10.1680/jstbu.20.00042

Web-flange distortional buckling analysis of partially restrained cold-formed steel beams under uplift loading

Zhenlei Chen,[a] Juan Zhao,[b,c] Long-yuan Li[c]

a) Faculty of Maritime and Transportation, Ningbo University, Ningbo, P. R. China
b) College of Urban Construction and Safety Engineering, Shanghai Institute of Technology, Shanghai, China
c) School of Engineering, Computing and Mathematics, University of Plymouth, Plymouth, UK

Abstract – Cold-formed steel members are usually used as purlins in buildings to support roof cladding and thus they can be treated as the restrained beams fully or partially in its lateral and torsional directions. However, when these beams are subjected to wind suction loading, their free flange is in compression, which may cause web-flange distortional buckling (WFDB). This paper presents an analytical study on the WFDB of zed-section purlins when subjected to uplift bending. A simplified model is proposed to describe the WFDB of partially restrained purlins, from which the formula for calculating the critical stress of the WFDB is derived. The present model is validated by the results obtained from the finite strip analysis.

Keywords: Mathematical modelling; Solid mechanics; Steel structures; Beams & girders; Buildings, structures & design.

1. Introduction

It is well known that beams made from cold-formed steel (CFS) can buckle in the form of local buckling (LB), distortional buckling (DB), or lateral-torsional buckling (LTB) (Hancock, 1978; Li, 2011; Selvaraj and Madhavan, 2019; Yerudkar and Vesmawala, 2018) because of their open-section and thin-thickness nature. In general, the design load of short-span CFS beams is controlled by the LB and DB; whereas that of long-span CFS beams is controlled mainly by the LTB. In literature, there are numerous studies reported on various buckling behaviors of CFS members (Cheng et al., 2015; Kwon et al., 2009; Mahi et al., 2019; Natesan and Madhavan, 2020; Wu et al., 2019), investigated by using experimental, numerical and/or analytical methods.

When the CFS beams are used in buildings, they are usually utilized as the secondary beams to support roof cladding. The typical sections used for such purpose are the channel-, sigma- and zed-sections, in which their upper flange is connected to cladding by self-tapping screw fasteners but their lower flange remains free. Under the action of gravity loading, the LTB behavior of the CFS beams can be improved significantly by their supported cladding, since the cladding gives some lateral and rotational restraints to the compressed flange (Gao and Moen, 2012; 2013a; 2013b). However, when the loading is in uplift direction, for instance, generated by a wind

suction, the free flange of the beams is in compression. In this case the LTB of the beams could still occur but their buckling mode is quite different from the conventional LTB mode of unrestrained beams (Li, 2004; Ye et al., 2002). Fig.1 displays the buckling curve and corresponding buckling modes of an upper flange-restrained zed-purlin under pure bending obtained from finite strip analysis. Owing to the restraints applied on the upper flange given by the cladding, the LTB mode of the purlin is now characterized by the translation and rotation of the element consisting of compressed flange and lip plus part of web close to the compressed flange and lip. This buckling occurs partly due to the flexibility of cladding in rotational direction and partly due to the deformability of the web, which allows the translation and rotation of the compressed element. To distinguish it from the conventional LTB, this buckling is named as web-flange distortional buckling (WFDB) (Hancock, 2003; Roger and Schuster, 1997). The WFDB of CFS beams has been investigated by several researchers, who tried to use the DB model to analyze the WFDB problem but was not success (Roger and Schuster, 1997). A few of analytical models were proposed (EN1993-1-3, 2006; Sokol, 1996; Svensson, 1985) to investigate the WFDB of CFS beams, in which the WFDB was modeled as the buckling of an axially compressed column on an elastic foundation. However, the reliability of these models was not fully demonstrated. Gao and Moen (2012) presented the mechanics-based expressions for predicting the rotational restraint provided by through-fastened metal panels to Z- and C-section purlins. The analytical equations include the effect of local panel deformation at a screw, and girt or purlin flange bending at a through-fastened connection. Later, they (Gao and Moen, 2013a) further investigated the flexural capacity of metal building wall systems with rigid board foam insulation sandwiched between C- and Z-section purlins. Vacuum box tests were conducted to simulate wind suction on the wall system and distinct failure modes were observed. Yuan et al. (2014) proposed a full section analytical model to investigate the WFDB of partially restrained CFS beams under uplift loading. The model is somewhat complicated and requires to solve a 3x3 eigenvalue matrix equation in order to obtain the critical stress. Recently, Luan and Li (2019) investigated the wind uplift capacity of single span Z-purlins supporting standing seam roof systems. Usefi et al. (2020) presented a nonlinear finite element analysis model on cold-formed steel wall panels to examine the failure modes of the hybrid wall panels. Raebel et al. (2020) carried out the experimental investigation into acceptable design methods for cold-formed metal deck by comparing the results of both the direct strength method and effective width method to experimental results for several metal deck profiles and gages.

In this paper we present an analytical model to describe the WFDB of partially restrained purlins when subjected to uplift loading. The formula for calculating the critical stress of the WFDB is derived. The present model is validated by using the results obtained from the finite strip analysis. The comparison of the predicted critical stresses with those obtained using finite strip analysis for various different size sections demonstrates the appropriateness and reliability of the proposed model.

2. Web-flange distortional buckling model

Consider a lipped zed-section purlin, which is to support a roof cladding used in the through fastened roof system where the flexibility of diaphragm is negligible (see Fig.2a). For the convenience, the cross-section dimensions of the purlin discussed herein do not consider the

bend radius and they are simply defined by its web depth *h*, flange width *b*, lip length *c*, and thickness *t*. It is believed that the difference induced by ignoring the bend radius would be negligible. When the purlin-sheeting through-fastened roof system is subjected to an uplift load, the load on the cladding is transferred to the purlin through the self-drilling screws and/or the contact between the cladding and upper flange. For a simply supported purlin under the action of the uplift loading, its upper flange is in tension and lower flange is in compression; the latter could induce a WFDB of a system involving the compressed flange, lip and part of the web, as shown in Fig.2b, in which the two rotational springs represent the rotational restraints provided by the cladding and web, respectively. Let x be the longitudinal axis, y and z be the cross-sectional axes parallel to the flange and web lines, respectively, as shown in Fig.2c. For the convenience of presentation, the origin of the coordinates is chosen at the centroid point of the unequal channel-section beam (see Fig.2c). When the WFDB occurs, the lateral and rotational displacements at point A are assumed to be v(x) and ϕ(x), as shown in Fig.2b. According to kinematic relations, the horizontal displacement, vertical displacement, and angle of twist of the unequal channel-section beam at the centroid point (point o) and shear centre (point s) can be expressed as follows,

$$v_o(x) = v - (d - z_D)\phi \tag{1}$$

$$w_o(x) = -y_D\phi \tag{2}$$

$$\phi_o(x) = \phi \tag{3}$$

$$v_s(x) = v - (d + z_s - z_D)\phi \tag{4}$$

$$w_s(x) = -(y_D - y_s)\phi \tag{5}$$

$$\phi_s(x) = \phi \tag{6}$$

where v_o, w_o, and ϕ_o are the horizontal displacement, vertical displacement, and angle of twist of the unequal channel-section beam at the centroid point, v_s, w_s, and ϕ_s are the horizontal displacement, vertical displacement, and angle of twist of the unequal channel-section beam at the shear centre, d is the length of the part of web (see Fig.2b) included in the buckling element, (y_D, z_D) and (y_s, z_s) are the coordinates of point D and point s in the yoz coordinate system (see Fig.2c).

The analysis of the axially compressed buckling of the unequal channel-section beam with elastic translational and rotational restraints defined by k_y and k_ϕ applied at point A (see Fig.2c) can be done by using traditional energy method. The strain energy of the unequal channel-section beam due to the buckling displacements expressed by Eqs.(1)-(6) can be calculated as follows,

$$U_b = \frac{1}{2}\int_o^l \left[EI_y\left(\frac{d^2w_s}{dx^2}\right)^2 + 2EI_{yz}\frac{d^2v_s}{dx^2}\frac{d^2w_s}{dx^2} + EI_z\left(\frac{d^2v_s}{dx^2}\right)^2 + GJ\left(\frac{d\phi_s}{dx}\right)^2 + EI_w\left(\frac{d^2\phi_s}{dx^2}\right)^2 \right] dx \tag{7}$$

where E is the Young's modulus, I_y, I_z and I_{yz} are the second moments and product moment of the cross-section area of the unequal channel section, G is the shear modulus, J is the torsion constant, and I_w is the warping constant.

The strain energy of the two elastic springs generated by the buckling displacements can be calculated as follows,

$$U_s = \frac{1}{2}\int_o^l k_\phi \left(\phi + \frac{v}{h-d}\right)^2 dx + \frac{1}{2}\int_o^l k_y v^2 dx \tag{8}$$

where k_y and k_ϕ are the equivalent stiffnesses of the translational and rotational springs applied at point A.

The work done by the pre-buckling axial stresses in the unequal channel-section beam can be calculated using the following formula (Alwis and Wang, 1996; Li, 2009; Li and Chen, 2008),

$$W = \frac{1}{2}\int_o^l N_o \left[\left(\frac{dv_o}{dx}\right)^2 + \left(\frac{dw_o}{dx}\right)^2 + \left(r_c \frac{d\phi}{dx}\right)^2\right] dx \tag{9}$$

where N_o is the axial compression force, which is the integration of the compression stress of the lower part of the cross-section as shown in Fig.2c, $r_c = \sqrt{(I_y + I_z)/A}$ is the polar radius of gyration of the unequal channel-section with respect to the centroid point, and $A=(b+c+d)t$ is the cross-sectional area of the unequal channel section.

Assume that when the WFDB occurs the lateral and rotational displacements of the unequal channel-section at point A can be approximately expressed as follows,

$$\phi(x) = A_k \sin\frac{k\pi x}{l} \tag{10}$$

$$v(x) = B_k \sin\frac{k\pi x}{l} \tag{11}$$

where A_k and B_k are the constants to be determined, l is the length of the beam, k is the half-wave number in the buckling mode, and l/k represents the actual half wavelength of the buckling mode. It is obvious that the displacements given in Eqs. (10) and (11) satisfy the simply supported end boundary conditions of the beam, i.e. $v(0) = v(l) = 0$ and $\phi(0) = \phi(l) = 0$. Substituting Eqs.(10) and (11) into (1)-(6) and then into (7)-(9), it yields,

$$U_b = \frac{l}{4}\left(\frac{k\pi}{l}\right)^4 \left\{\begin{array}{l} EI_y(y_D - y_s)^2 A_k^2 - 2EI_{yz}(y_D - y_s)A_k\left[B_k - (d + z_s - z_D)A_k\right] \\ \quad + EI_z\left(B_k - (d + z_s - z_D)A_k\right)^2 + GJ\left(\frac{l}{k\pi}\right)^2 A_k^2 + EI_w A_k^2 \end{array}\right\} \tag{12}$$

$$U_s = \frac{l}{4}\left[k_\phi\left(A_k + \frac{B_k}{h-d}\right)^2 + k_y B_k^2\right] \tag{13}$$

$$W = \frac{N_o l}{4}\left(\frac{k\pi}{l}\right)^2 \left[\left(B_k - (d - z_D)A_k\right)^2 + y_D^2 A_k^2 + r_c^2 A_k^2\right] \tag{14}$$

The stationary condition of the total potential when buckling occurs requires that $\delta^2\Pi=\delta^2(U_b+U_s-W)=0$. The critical load thus can be obtained by solving for the smallest eigenvalue of the following determinant:

$$\begin{Vmatrix} \dfrac{\partial^2\Pi}{\partial A_k^2} & \dfrac{\partial^2\Pi}{\partial A_k \partial B_k} \\ \dfrac{\partial^2\Pi}{\partial A_k \partial B_k} & \dfrac{\partial^2\Pi}{\partial B_k^2} \end{Vmatrix} = \begin{Vmatrix} a_{11} - N_o b_{11} & a_{12} - N_o b_{12} \\ a_{12} - N_o b_{12} & a_{22} - N_o b_{22} \end{Vmatrix} = 0 \tag{15}$$

in which,

$$a_{11} = \left(\frac{k\pi}{l}\right)^2 E\left[I_y (y_D - y_s)^2 + 2I_{yz}(y_D - y_s)(d + z_s - z_D) + I_z (d + z_s - z_D)^2 + EI_w\right] + GJ + \left(\frac{l}{k\pi}\right)^2 k_\phi$$

$$a_{12} = -\left(\frac{k\pi}{l}\right)^2 E\left[I_{yz}(y_D - y_s) + I_z (d + z_s - z_D)\right] + \left(\frac{l}{k\pi}\right)^2 \frac{k_\phi}{h - d},$$

$$a_{22} = \left(\frac{k\pi}{l}\right)^2 EI_z + \left(\frac{l}{k\pi}\right)^2 \left(\frac{k_\phi}{(h-d)^2} + k_y\right),$$

$$b_{11} = (d - z_D)^2 + y_D^2 + r_c^2,\ b_{12} = -(d - z_D),\ b_{22} = 1$$

The smallest eigenvalue of Eq.(15) can be expressed as follows,

$$N_o = \frac{(a_{11}b_{22} + a_{22}b_{11} - 2a_{12}b_{12}) - \sqrt{(a_{11}b_{22} + a_{22}b_{11} - 2a_{12}b_{12})^2 - 4(a_{11}a_{22} - a_{12}^2)(b_{11}b_{22} - b_{12}^2)}}{2(b_{11}b_{22} - b_{12}^2)} \tag{16}$$

For a given half wavelength $\lambda = l/k$, one can calculate the critical load N_o from Eq.(16). After the critical load N_o is obtained, the following critical stress in the compressed flange can be obtained,

$$\sigma_{cr} = \frac{N_o}{(c + b + d)t - (c^2 + d^2)t/h} \tag{17}$$

where σ_{cr} is the critical stress in the compressed flange when the beam has a WFDB. Eq.(17) gives the critical stress of WFDB of purlins used in through-fastened systems with rigid diaphragm where the effect of rotational flexibility of sheathing connection on the pre-buckling stress distribution is ignored.

3. Determination of sectional properties

The evaluation of the total potential of the unequal channel-section beam requires the sectional properties of the unequal channel. This section provides the derivation of the formulas used to calculate the sectional properties required. Note that, the coordinates of points D and B in the present yoz coordinate system (see Fig.3a) can be expressed as follows,

$$y_D = \frac{b(2c + b)}{2(d + b + c)} \tag{18}$$

$$z_D = \frac{c^2 + d^2}{2(d + b + c)} \tag{19}$$

$$y_B = y_D - b = -\frac{b(2d + b)}{2(d + b + c)} \tag{20}$$

$$z_B = z_D - c = \frac{d^2 - c(2d + 2b + c)}{2(d + b + c)} \tag{21}$$

where b, c, and d are the dimensions of the unequal channel section (see Fig.3a), (y_D, z_D) and (y_B, z_B) are the coordinates of points D and B in the yoz coordinate system, respectively. The second moments of area about the two axes and the product moment of area thus can be calculated as follows,

$$I_y = \frac{c^3 t}{12} + ct\left(\frac{c}{2} - z_D\right)^2 + \frac{d^3 t}{12} + dt\left(\frac{d}{2} - z_D\right)^2 + btz_D^2 \tag{22}$$

$$I_z = \frac{b^3 t}{12} + bt\left(\frac{b}{2} - y_D\right)^2 + ct(b - y_D)^2 + dty_D^2 \tag{23}$$

$$I_{yz} = dty_D\left(z_D - \frac{d}{2}\right) + btz_D\left(y_D - \frac{b}{2}\right) + ct(b - y_D)\left(\frac{c}{2} - z_D\right) \tag{24}$$

where I_y and I_z are the second moments of area about y- and z-axis, respectively, I_{yz} is the product moment of area, and t is the thickness. Let Y and Z be the two principal coordinate axes (see Fig.3b). The angle between y and Y axes or between z and Z axes can be calculated as follows,

$$\tan 2\theta = -\frac{2I_{yz}}{I_z - I_y} \tag{25}$$

The second moments of area about the two principal axes thus can be calculated as follows,

$$I_{YY} = I_y - (1 - \cos 2\theta)\sqrt{\left(\frac{I_z - I_y}{2}\right)^2 + I_{yz}^2} \tag{26}$$

$$I_{ZZ} = I_z + (1 - \cos 2\theta)\sqrt{\left(\frac{I_z - I_y}{2}\right)^2 + I_{yz}^2} \tag{27}$$

where I_{YY} and I_{ZZ} are the second moments of area about Y- and Z-axis, respectively. The coordinates of points B and D in the principal coordinate system can be expressed as,

$$Y_B = y_B \cos\theta - z_B \sin\theta = -\frac{b(2d + b)}{2(d + b + c)}\cos\theta - \frac{d^2 - c(2d + 2b + c)}{2(d + b + c)}\sin\theta \tag{28}$$

$$Z_B = y_B \sin\theta + z_B \cos\theta = -\frac{b(2d + b)}{2(d + b + c)}\sin\theta + \frac{d^2 - c(2d + 2b + c)}{2(d + b + c)}\cos\theta \tag{29}$$

$$Y_D = y_D \cos\theta - z_D \sin\theta = \frac{b(2c + b)}{2(d + b + c)}\cos\theta - \frac{c^2 + d^2}{2(d + b + c)}\sin\theta \tag{30}$$

$$Z_D = y_D \sin\theta + z_D \cos\theta = \frac{b(2c + b)}{2(d + b + c)}\sin\theta + \frac{c^2 + d^2}{2(d + b + c)}\cos\theta \tag{31}$$

where (Y_B, Z_B) and (Y_D, Z_D) are the coordinates of points B and D in the YoZ coordinate system, respectively. When the section is subjected to a load P_Y parallel to Y-axis, the twisting moment of P_Y about point D should be equal to the twist moment created by the shear flow in the element away from Point D. The latter can be calculated as follows (see Fig.3c),

$$M_\tau = \int_o^c \frac{bP_Y}{I_{ZZ}} ts\left(|Y_B| + \frac{s}{2}\sin\theta\right)ds = \frac{P_Y btc^2}{2I_{ZZ}}\left(|Y_B| + \frac{c}{3}\sin\theta\right) \quad (32)$$

Let (Y_s, Z_s) be the coordinates of shear centre *s* in the YoZ coordinate system. Thus,

$$Z_s = \frac{M_\tau}{P_Y} + Z_D = \frac{btc^2}{2I_{ZZ}}\left(|Y_B| + \frac{c}{3}\sin\theta\right) + Z_D \quad (33)$$

Similarly, when the section is subjected to a load P_Z parallel to *Z*-axis, the twisting moment of P_Z about point D should be equal to the twist moment created by the shear flow in the element away from point D. The latter can be calculated as follows (see Fig.3d),

$$M_\tau = \int_o^c \frac{bP_Z}{I_{YY}} ts\left(|Z_B| - \frac{s}{2}\cos\theta\right)ds = \frac{P_Z btc^2}{2I_{YY}}\left(|Z_B| - \frac{c}{3}\cos\theta\right) \quad (34)$$

Thus,

$$Y_s = Y_D - \frac{M_\tau}{P_Z} = Y_D - \frac{btc^2}{2I_{YY}}\left(|Z_B| - \frac{c}{3}\cos\theta\right) \quad (35)$$

The coordinates of the shear centre *s* in the yoz coordinate system thus can be obtained by follows,

$$y_s = Y_s\cos\theta + Z_s\sin\theta \quad (36)$$

$$z_s = -Y_s\sin\theta + Z_s\cos\theta \quad (37)$$

where (y_s, z_s) are the coordinates of the shear centre in the yoz coordinate system. The warping function of the unequal channel section can be expressed as follows,

$$\omega_s = \int_o^s r ds = \int_o^s (y_s - y_B)ds = (y_s - y_B)s \qquad 0 \le s \le c \quad (38)$$

$$\omega_s = (y_s - y_B)c - \int_c^s r ds = (y_s - y_B)c - \int_c^s (z_s - z_D)ds = (y_s - y_B)c - (z_s - z_D)(s - c)$$

$$c \le s \le c + b \quad (39)$$

$$\omega_s = (y_s - y_B)c - z_s b + \int_{c+b}^s r ds = (y_s - y_B)c - (z_s - z_D)b + \int_{c+b}^s (y_D - y_s)ds$$

$$= (y_s - y_B)c - (z_s - z_D)b + (y_D - y_s)(s - c - b)$$

$$c + b \le s \le c + b + d \quad (40)$$

The average value of the warping function can be obtained by follows,

$$\begin{aligned}\overline{\omega}_s &= \frac{1}{c+b+d}\int_o^s \omega_s ds = \frac{1}{c+b+d}\int_o^c (y_s - y_B) s ds \\ &+ \frac{1}{c+b+d}\int_c^{c+b}\left[(y_s - y_B)c - (z_s - z_D)(s-c)\right]ds \\ &+ \frac{1}{c+b+d}\int_{c+b}^{c+b+d}\left[(y_s - y_B)c - (z_s - z_D)b + (y_D - y_s)(s-c-b)\right]ds \\ &= (y_s - y_B)c + \frac{(y_D - y_s)d^2 - (y_s - y_B)c^2}{2(c+b+d)} - \frac{(b+2d)(z_s - z_D)b}{2(c+b+d)}\end{aligned} \tag{41}$$

The warping constant thus can be calculated as follows,

$$\begin{aligned}I_\omega &= \int_o^{c+b+d}(\overline{\omega}_s - \omega_s)^2 t ds = t\int_o^{c+b+d}(\omega_s^2 - \overline{\omega}_s^2)ds = \frac{t(y_s - y_B)^2 c^3}{3} + \frac{t(z_s - z_D)^2 b^3}{12} + \frac{t(y_D - y_s)^2 d^3}{12} \\ &+ tb\left[c(y_s - y_B) - \frac{b(z_s - z_D)}{2}\right]^2 + td\left[c(y_s - y_B) - b(z_s - z_D) + \frac{d(y_D - y_s)}{2}\right]^2 - t\overline{\omega}_s^2(c+b+d)\end{aligned} \tag{42}$$

The torsion constant can be expressed as follows,

$$J = \frac{(d+c+b)t^3}{3} \tag{43}$$

Eqs.(22), (23), (24), (42) and (43) can be used to calculate the second moments, product moment, warping constant and torsion constant of the cross-section area of the unequal channel section.

4. Numerical examples

Before the critical stress of WFDB can be calculated by using the present model described above for a partially rotationally restrained purlin, we have to know the spring constants k_y and k_ϕ, and the length d of the partial web involved in the WFDB model (see Fig.2c). Note that both k_y and k_ϕ are dependent not only on the rotational spring stiffness of the cladding k_{sh} but also on the deformability of the web. In theory, if the shape and dimensions of the cladding and purlin are known, then k_ϕ and k_y can be calculated. In the following numerical examples, three different values are employed for k_{sh}, representing three different types of cladding, namely weak (k_{sh}=10^{-5}D/h), medium (k_{sh}=0.25D/h) and strong (k_{sh}=D/h) cladding. The values for k_y and k_ϕ are taken as k_y=k_{sh}/(h-d)2 and k_ϕ=[D/(h-d)-k_{sh}]b/h, where D=$Et^3/[12(1-\nu^2)]$ is the flexural rigidity of the web plate. The value of d is taken as d=h/5, which was determined through the trial-error analysis of the critical stresses obtained from the present model and those predicted using the finite strip analysis program (CUFSM Version 2.6) developed originally by Schafer (1997) and Schafer et al. (2010) for 59 zed-section purlins of different sizes manufactured by Albion Sections in the UK. Note that in Eurocode (EN1993-1-3, 2006) d=h/5 was also recommended for calculating the critical stress of WFDB. However, the model used in Eurocode involves only the translational

spring that is applied at the compressed flange. To demonstrate the present model, the critical stresses of WFDB for three different size purlins (see Table 1) obtained from the present model are compared with those predicted using the finite strip method and are shown in Figs.4-6 for the three types of cladding, respectively. In the finite strip method the full section shown in Fig.2a is modelled and the rotational spring representing the cladding restraint is applied at the junction between the web and upper flange. It is evident from the comparison shown in Figs.4-6 that the calculated critical stress from the present model is in very good agreement with that predicted by using the finite strip method. The difference between them is observed only at the beginning of the curves where the critical stress is very high and the corresponding half wavelength is very short.

The critical stresses shown in Fig.4 are for the purlins with a weak restraint from the cladding. It can be seen from the figure that the critical stress of WFDB for all of the three size sections decreases continuously with the increase of purlin length, which is very similar to the critical stress of LTB of the beam. In fact, when the cladding has a weak rotational restraint to the purlin, the WFDB mode of the purlin becomes very close to the torsional buckling mode of the beam. This indicates that the present model can also be used to predict the critical stress of LTB of the beam although the model itself consists of only one lip, one flange and part of the web. Also, as it is to be expected, the critical stress is higher in the larger section for the same purlin length or the same half wavelength. A parametric study on k_ϕ shows that, when k_{sh} is small the critical stress of WFDB seems insensitive to k_ϕ provided that k_ϕ is about or greater than Db/[h(h-d)]. This further demonstrates that when k_{sh} is small the WFDB mode tends to the LTB mode.

Fig.5 shows the critical stresses of WFDB of the three purlins restrained by a medium cladding. It can be observed from the figure that the critical stress initially decreases with the increased purlin length until it reaches to the minimum point. After that minimum point the critical stress recovers slightly. It is interesting to note that, the smaller the section, the higher the minimum critical stress. The half wavelength at the minimum critical stress point is found to be shorter in the smaller size purlin. This indicates that the cladding has more influence on the buckling of smaller section purlin. Note that the half wavelength at the minimum critical stress point is about 4.2 m, 5.5 m, and 7.5 m for the small, medium and large size sections, respectively. Given the fact that the largest span length of purlins is about 7 m for small sections, 9 m for medium sections, and 12 m for large sections, the half wavelengths shown in Fig.5 could also be treated as the beam length.

Fig.6 shows the critical stresses of WFDB of the three size section purlins restrained by a strong cladding. It can be seen from the figure that all of the three critical stress curves exhibit a parabolic shape with a clearly defined minimum point. The minimum critical stress is found much higher in the small size section than in the large size section; whereas its corresponding half wavelength is found to be shorter in the small size section than in the large size section. The half wavelengths at the three minimum critical stress points shown in Fig.6 are about 3 m, 4.5 m and 5.5 m, which are all smaller than those shown in Fig.5. The short half wavelength means that the purlin could buckle in a mode with multiple waves. For instance, a 7 m long medium size section purlin is likely to buckle in the mode of two waves (each has 3.5 m half wavelength) with the critical stress of about $0.5\sigma_y$ rather than in the mode of a single wave (7.0 m half wavelength) with the critical stress of about $0.62\sigma_y$.

5. Conclusions

In this paper, an analytical model has been developed for describing the WFDB of partially rotationally restrained zed-purlins, used in the fastened sheathing systems with rigid diaphragm. The formula for calculating the critical stress of WFDB has been derived based on the present model. The model has been validated using the finite strip analysis method for a wide range of purlin sizes. From the results obtained the following conclusions can be drawn:

- The WFDB of partially rotationally restrained zed-purlins can be modelled by using a system consisting of the compressed flange, lip and part of web. The length of the partial web involved in the WFDB model can be taken as one-fifth of the web depth.
- The effect of cladding rotational restraint and the distortional flexibility of the section itself on the WFDB of purlins can be modelled using a translational spring and a rotational spring applied at the cutting point of the web.
- The translational spring stiffness can be expressed in terms of the cladding rotational spring stiffness; while the rotational spring stiffness is found to be dependent not only on the web flexural stiffness but also the cladding rotational spring stiffness.
- For weak restraint cladding, the critical stress of WFDB is found to decrease continuously with the increase of beam length, which is similar to that of LTB of the beams.
- For medium and strong restraint cladding, the critical stress of WFDB is found to initially decrease with the increased half wavelength until it reaches to a minimum point. After that point the critical stress starts to increase with increased half wavelength. The critical stress and corresponding half wavelength at the minimum point are heavily dependent on the rotational spring stiffness of the cladding.

References

Alwis WA and Wang CM (1996) Wagner term in flexural-torsional buckling of thin-walled open-profile columns. Engineering Structures **18(2)**: 125-132.

Cheng SS, Li LY and Kim B (2015) Buckling analysis of cold-formed steel channel-section beams at elevated temperatures. Journal of Constructional Steel Research **104**: 74-80.

EN1993-1-3 (2006) Eurocode 3 – Design of Steel Structures – Part 1-3: General rules – Supplementary rules for cold-formed members and sheeting. BSI.

Gao T and Moen CD (2012) Predicting rotational restraint provided to wall girts and roof purlins by through-fastened metal panels. Thin-Walled Structures **61**: 145-153.

Gao T and Moen CD (2013a) Flexural strength experiments on exterior metal building wall assemblies with rigid insulation. Journal of Constructional Steel Research **81**: 104-113.

Gao T and Moen CD (2013b) Extending the Direct Strength Method for cold-formed steel design to through-fastened simple span girts and purlins with laterally unbraced compression flanges. Journal of Structural Engineering **104(6)**: 1299–1328.

Hancock GJ (1978) Local, distortional and lateral buckling of I-beams. Journal of Structural Division (ASCE) **104(11)**: 1787–1798.

Hancock GJ (2003) Cold-formed steel structures. Journal of Constructional Steel Research **59(4)**: 473–87.

Kwon YB, Kim BS and Hancock GJ (2009) Compression tests of high strength cold-formed steel channels with buckling interaction. Journal of Constructional Steel Research **65(2)**: 278-289.

Li LY (2004) Lateral-torsion buckling of cold-formed zed-purlins partial-laterally restrained by metal sheeting. Thin-Walled Structures **42(7)**: 995-1011.

Li LY (2009) Analyses of distortional buckling of cold-formed sigma purlins using EN 1993-1-3. Journal of Constructional Steel Research **65(12)**: 2099–2102.

Li LY (2011) Calculation of moment capacity of cold-formed steel members. International Journal of Structural Engineering **2(2)**: 101–15.

Li LY and Chen JK (2008) An analytical model for analyzing distortional buckling of cold-formed steel sections. Thin-Walled Structures **46(12)**: 1430–1436.

Luan W and Li YQ (2019) Experimental investigation on wind uplift capacity of single span Z-purlins supporting standing seam roof systems, Thin-Walled Structures **144**: 106324.

Mahi I, Djelil M, Djafour N and Djafour M (2019) Calculation of critical load for pure distortional buckling of lipped channel columns. Periodica Polytechnica Civil Engineering **63(4)**: 1016-1029.

Natesan V and Madhavan M (2020) Experimental study of clip angle bolted connection between two cold-formed steel channels. Proceedings of the Institution of Civil Engineers - Structures and Buildings **173(9)**: 672-689.

Raebel CH, Schultz JA and Whitsell B (2020) Experimental investigation into acceptable design methods for cold-formed metal deck. Journal of Constructional Steel Research **172**: 106176.

Roger CA and Schuster RM (1997) Flange/web distortional buck-ling of cold-formed steel sections in bending. Thin-Walled Structures **27(1)**: 13-29.

Schafer BW (1997) Cold-formed steel behavior and design: Analytical and numerical modeling of elements and members with longitudinal stiffeners. PhD thesis, Cornell University, Ithaca, USA.

Schafer BW, Li Z and Moen CD (2010) Computational modelling of cold-formed steel. Thin Walled Structures **48(10–11)**: 752-762.

Selvaraj S and Madhavan M (2019) Structural design of cold-formed steel face-to-face connected built-up beams using direct strength method. Journal of Constructional Steel Research **160**: 613-628.

Sokol L (1996) Stability of cold formed purlins braced by steel sheeting. Thin-Walled Structures **25(4)**: 247-268.

Svensson SE (1985) Lateral buckling of beams analysed as elastically supported columns subject to a varying axial force. Journal of Constructional Steel Research **5(3)**: 179-193.

Usefi N, Ronagh H and Sharafi P (2020) Numerical modelling and design of hybrid cold-formed steel wall panels. Thin-Walled Structures **157**: 107084.

Wu MJ, Huang X and Zhu J (2019) Distortional buckling of a CFS channel section with and without stiffened flanges. Journal of Mechanical Science and Technology **33(6)**: 2623–2632.

Ye ZM, Kettle R, Li LY and Schafer BW (2002) Buckling behaviour of cold-formed zed-purlins partially restrained by steel sheeting. Thin-walled Structures **40(10)**: 853-864.

Yerudkar DS and Vesmawala GR (2018) Strength and buckling of cold-formed steel laterally unbraced stiffened C and Z sections. Proceedings of the Institution of Civil Engineers - Structures and Buildings **171(3)**: 216-225.

Yuan WB, Cheng SS, Li LY and Kim B (2014) Web-flange distortional buckling of partially restrained cold-formed steel purlins under uplift loading. International Journal of Mechanical Science **89**: 476–481.

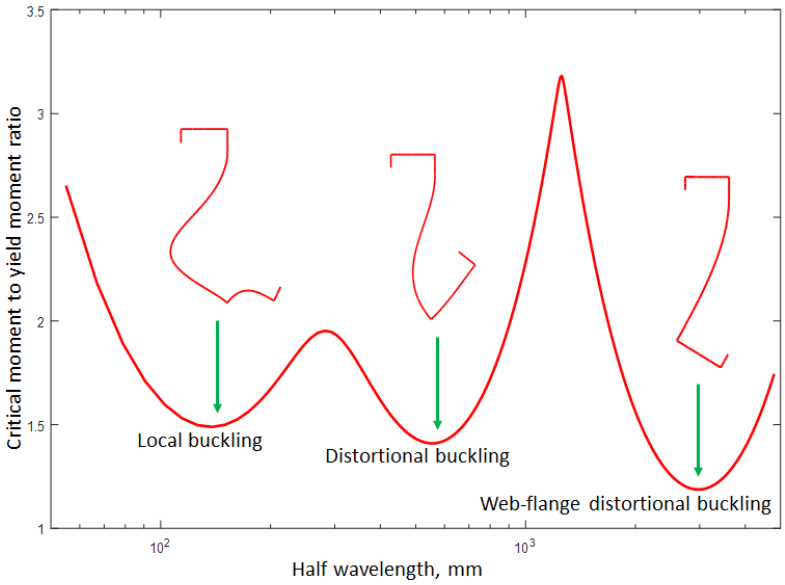

Figure 1. Critical moment and corresponding buckling modes of an upper flange-restrained zed-purlin under pure bending (web depth h=250 mm, flange width b=70 mm, lip length c=20 mm, thickness t=2.5 mm, yield strength σ_y=390 MPa).

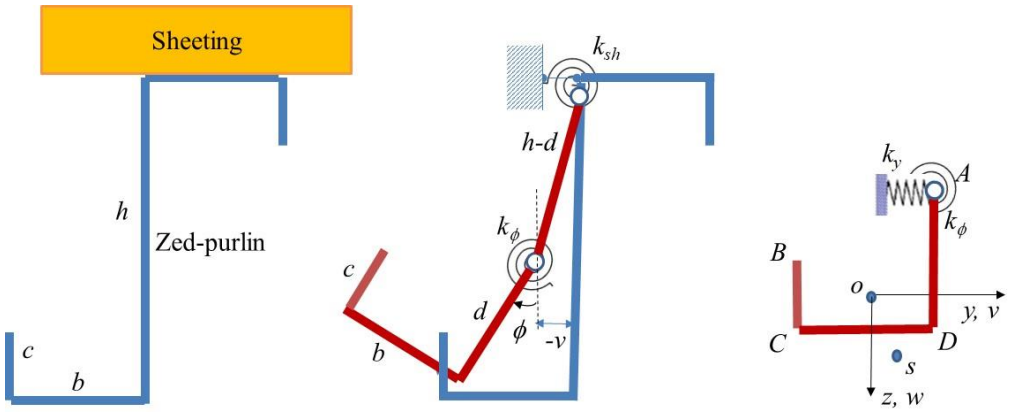

(a) (b) (c)

Figure 2. Web-flange distortional buckling analysis model. (a) Zed-purlin sheeting system. (b) Buckling of compressed web-flange-lip system. (c) Buckling element consisting of compressed flange, lip and part of web (o is the centroid point
and s is shear centre of the unequal channel-section ABCD).

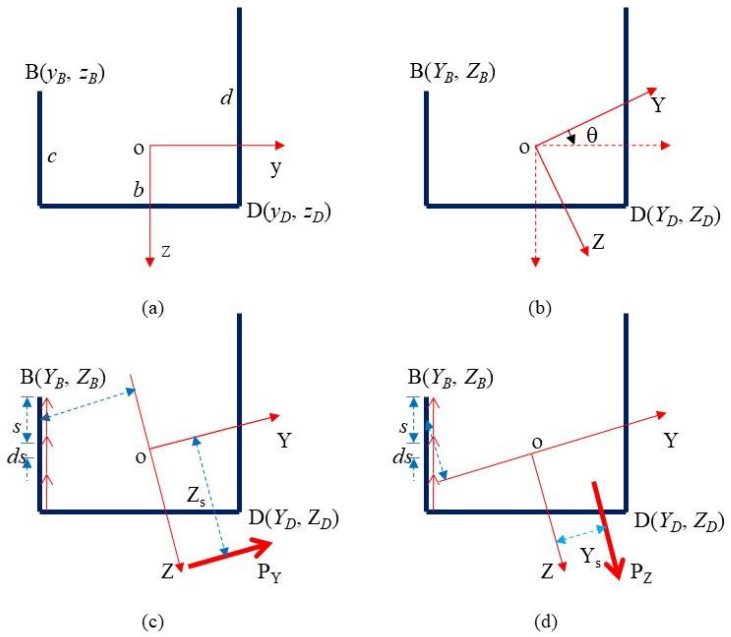

Figure 3. (a) Section dimensions. (b) Principal axes. (c) Shear centre due to a load parallel to Y-axis. (d) Shear centre due to a load parallel to Z-axis.

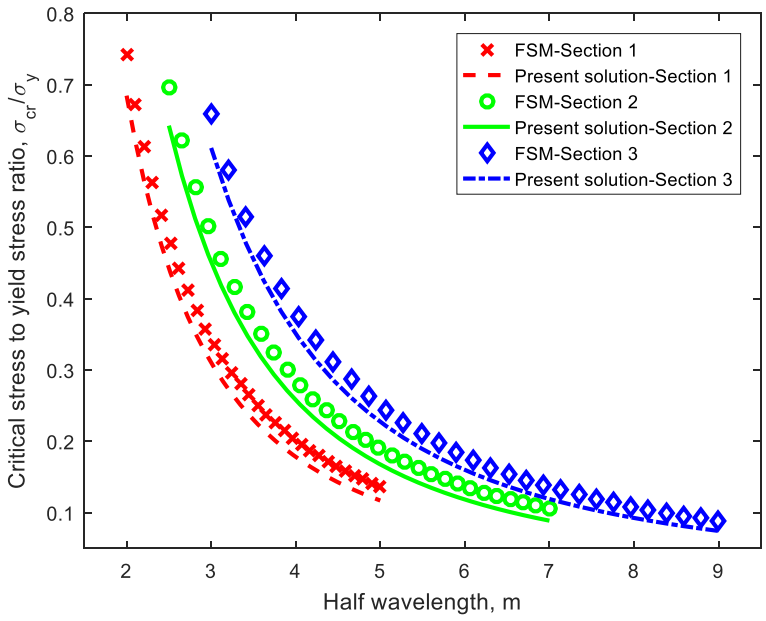

Figure 4. Variation of critical stress of web-flange distortional buckling with half-wavelength for weak sheeting with $k_{sh}=10^{-5}D/h$ (E=210 GPa, ν=0.3, σ_y=390 MPa).

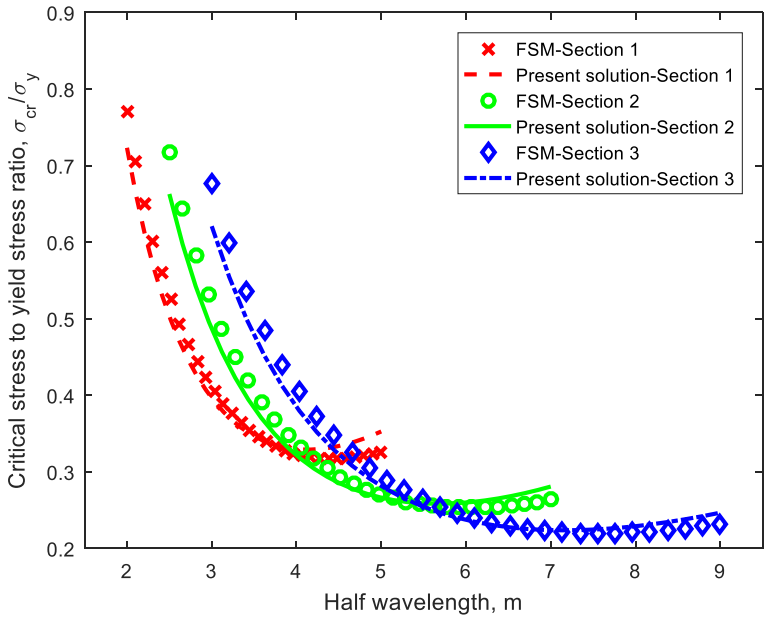

Figure 5. Variation of critical stress of web-flange distortional buckling with half-wavelength for medium sheeting with k_{sh}=0.25D/h (E=210 GPa, ν=0.3, σ_y=390 MPa).

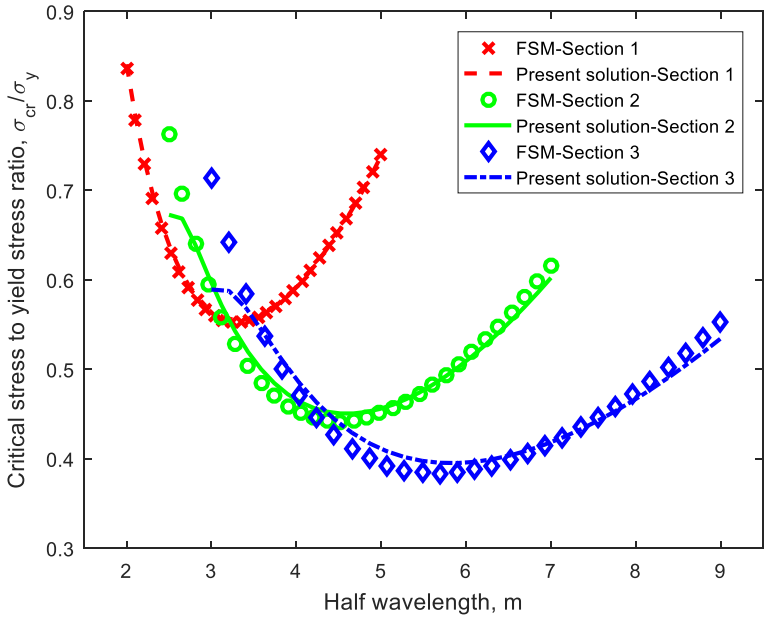

Figure 6. Variation of critical stress of web-flange distortional buckling with half-wavelength for strong sheeting with k_{sh}=D/h (E=210 GPa, ν=0.3, σ_y=390 MPa).

Table 1. Dimensions of sections used in numerical examples (unit: mm)

Section	Section depth *h*	Flange width *b*	Lip length *c*	Thickness *t*
No.1	150	50	15	1.5
No.2	225	60	20	2.0
No.3	300	70	30	2.5